

The effect of carbon fiber content on physico-mechanical properties of recycled poly(ethylene terephthalate) composites additively manufactured with fused filament fabrication

Amalia Katalagarianakis^{1,3,°}, Babs Van de Voorde^{2,3,°}, Nele Pien^{2,3}, Efstratios Polyzos¹, Ivica Duretek⁴, Clemens Holzer⁴, Ludwig Cardon⁵, Katrien V. Bernaerts⁶, Danny Van Hemelrijck¹, Sandra Van Vlierberghe², Lincy Pyl^{1*}

¹ Department of Mechanics of Materials and Constructions (MeMC), Vrije Universiteit Brussel, Pleinlaan 2, B-1050 Brussels, Belgium

² Department of Organic and Macromolecular Chemistry, Centre of Macromolecular Chemistry (CMaC), Polymer Chemistry and Biomaterials Group (PBM), Ghent University, Krijgslaan 281 S4-bis, B-9000 Ghent, Belgium

³ SIM vzw, Technologiepark 48, BE-9052 Zwijnaarde, Belgium

⁴ Chair of Polymer Processing, Montanuniversität Leoben, Otto Glöckel-Straße 2, 8700 Leoben, Austria

⁵ Department of Materials, Textiles and Chemical Engineering, Centre for Polymer and Material Technologies (CPMT), Ghent University, Technologiepark 130, BE-9052 Zwijnaarde, Belgium

⁶ Aachen-Maastricht Institute for Biobased Materials (AMIBM), Maastricht University, Urmonderbaan 22, 6167RD Geleen, the Netherlands

* Lincy.Pyl@vub.be

° Both authors contributed equally

Abstract

The combination of recycled fiber reinforcement with recycled polymer as a feedstock material for extrusion-based additive manufacturing creates an opportunity for a more sustainable material use. In this study, recycled short carbon fibers were combined with recycled poly(ethylene terephthalate) (PET) to obtain carbon fiber-reinforced PET filaments via melt extrusion. The carbon fiber content of the extruded filaments ranged from 0.4 to 40.7 wt%. The molar mass and the degree of crystallinity after processing were determined to evaluate the influence of the extrusion process on the physico-chemical and mechanical properties of the reinforced PET filaments. Furthermore, pressure-volume-temperature measurements were carried out to investigate the influence of the carbon fibers on the shrinkage of the semi-crystalline PET. Samples were printed and their superior mechanical properties, including a 390 % increase in tensile modulus, were confirmed via tensile testing. Analysis via X-ray micro-computed tomography indicated that the fiber length reduced with increasing fiber content. The high degree of fiber alignment that was observed in the extruded filaments, was slightly reduced after deposition. Scanning electron microscopy data showed that fiber pull-out was the governing failure mechanism, indicating a weak interface between the carbon fibers and the matrix. The results show the potential of extrusion-based additive manufacturing to valorize recycled PET and recycled carbon fibers.

Keywords: Recycled poly(ethylene terephthalate), recycled carbon fibers, melt extrusion, fused filament fabrication, mechanical properties, shrinkage

1. Introduction

Poly(ethylene terephthalate) (PET) is an indispensable and versatile polymer widely used for the production of beverage bottles, (non-)food packaging, technical parts and synthetic fibers for textiles.[1–3] Being one of the most common thermoplastics, it owes its popularity to excellent chemical and mechanical properties, while being lightweight.[4] For example, PET shows high thermal stability and has a semi-crystalline microstructure, providing high stiffness and strength. However, the increasing consumption of PET worldwide raises concerns about its environmental impact. In 2019, the European demand for PET reached nearly 4 million tons, which were mainly used for synthetic fiber and bottle production.[5] Due to its large volume fraction in polymer waste streams and its chemical resistance, wide-scale PET reclamation and recycling programs have already been

successfully established.[6] Widespread use of recycled PET (rPET) would contribute to the circularity goals of the European Commission for resource-efficiency and sustainability as PET products can consist of up to 100 % recycled content.[7] In 2020, the global market for rPET was valued at USD 8.6 billion and it is expected to increase with 6.7 % every year between 2021 and 2028.[8] Moreover, the dominant end-user market for rPET was synthetic fibers with a value of 44 %, while food packaging accounted for nearly 20 %.

One of the processing techniques which could also contribute to extending the lifetime of recycled materials is extrusion-based additive manufacturing or fused filament fabrication (FFF).[9,10] FFF is one of the most widely used three-dimensional (3D) printing techniques, owing its success to its simplicity and relatively low cost. FFF allows the manufacturing of polymer parts with complex shapes in a layer-by-layer fashion according to a computer-aided design (CAD), without the use of expensive molds and while minimizing material waste.[11] The technique is traditionally used for rapid-prototyping of on-demand products and other applications for which low to medium volumes are manufactured.[12] Due to the possibility to create intricate and complex geometries, the application field of the FFF technique has broadened towards functional parts in automotive [13], aerospace [14,15] and biomedical industries [16].

Recycled PET has been shown to be suitable as polymer feedstock for FFF, despite its high melting temperature, water absorption and semi-crystallinity which can all reduce printability.[17] A crucial processing step in the extrusion of PET for FFF feedstock is the drying of PET pellets. Drying was found to be crucial to obtain a uniform filament diameter as it led to an increased viscosity. Drying also played a role in the printing process, where a low moisture content reduced the occurrence of voids or bubbles that can lead to a reduced mechanical performance. Furthermore, a controllable degree of crystallinity of printed parts is desirable as it is shown to affect tensile modulus and strength.[18] The degree of crystallinity of rPET is reported to be dependent on molecular weight of the polymer and the cooling rate.[17,19] The recycling of PET has been reported to not affect mechanical properties and print accuracy when compared to virgin material.[20] As FFF printed parts can be prone to high void contents due to the way the printer deposits the extruded filament, possibly generating air gaps in between tracks, the void content in rPET samples has also been investigated. The build plate, heated above the glass transition temperature at 100°C, was shown to have an annealing effect on the sample causing the absence of voids in the bottom layers and a gradually increasing presence of small voids towards the top layers.

While the FFF printing technique allows selection from a broad range of materials and material properties, its inherent weaknesses still cast a shadow over the mechanical performance of FFF printed parts. FFF printed thermoplastic parts have been mostly used for nonstructural and low-performance applications, as the naturally weak tensile properties of thermoplastic polymers do not suffice for structural parts.[21,22] This significant limitation has driven researchers towards the reinforcement of the thermoplastic filaments with additives such as short carbon fibers (CFs). The mechanical performance of carbon fiber-reinforced (CFR) acrylonitrile butadiene styrene (ABS), polylactic acid (PLA), poly(ethylene terephthalate glycol) (PETG), polyamide (PA) and polyetherimide (PEI) manufactured with FFF has already been investigated in recent years.[11,23–25]

Previous work has shown that fibers align with the printing direction due to the flow-induced orientation of the fibers.[24,26–29] Alignment of the fibers with the loading direction has a large impact on both the tensile modulus and strength.[21,23,30,31] For example, the addition of 30 wt% short CFs (0.2 – 0.4 mm) to an ABS matrix resulted in an increase of approximately 700 % in tensile modulus and approximately 115 % in tensile strength due to the high alignment of the fibers with the loading direction.[24] A maximum fiber content of 40 wt% was reported, above which the printing

nozzle clogged. For 18 wt% of 73 μm long CF incorporated in PETG, an improvement of 313 % in tensile modulus and 48 % in tensile strength was observed.[25] The drastic improvement of the mechanical properties of the printed part due to the fibers widens the possibilities for the use of CFR thermoplastics.[22] Carbon fibers can also reduce void formation in FFF printed parts both between layers and in between tracks. The former by increasing the thermal conductivity and improving the fusion between layers, and the latter by improving the packing of the tracks.[20] However, an increasing number of fiber ends can also cause the formation of voids inside the tracks themselves.[21]

To benefit from the reinforcing characteristics of the carbon fibers, reductions in fiber length during processing should be avoided. However, significant drops in fiber length have already been noticed due to the high-shear mixing step in the compounding and the printing process itself.[32] This fiber damage during processing currently limits the use of discontinuous CFR thermoplastic materials as their mechanical performance does not compare to aircraft aluminum yet.[11] Blok *et al.* concluded that fibers used to reinforce polymer FFF filaments should be above a critical length, namely 0.78 mm and 0.8 - 1.38 mm for CF in a PA and PLA matrix respectively.[33]

Besides improving the mechanical properties, carbon fibers also reduce distortion of the printed part by increasing thermal conductivity and decreasing the coefficient of thermal expansion.[21] Semi-crystalline thermoplastics suffer from shrinkage and warpage due to their crystallization during cooling.[34] When the deposited thermoplastic cools down, the free volume decreases, which is more pronounced for semi-crystalline materials compared to amorphous materials as the formed crystals are denser. As this can be problematic for parts that require a high dimensional accuracy, the prevention of shrinkage and warpage by incorporating fillers in the feedstock polymer has already been described in literature.[21,35–39]

In addition to the fibers themselves, also the printer settings play a role in the quality of the printed composite. For example, control of cooling conditions during printing is essential for a sufficient bond quality between adjacent tracks, which will reflect in the mechanical properties of the printed parts.[12]

While research towards the use of recycled PET as feedstock for FFF has already been reported [17,40,41], studies on reinforcing the polymer with carbon fibers are currently lacking. Carbon fibers show potential to significantly improve the mechanical properties and reduce the amount of shrinkage and warpage of printed parts. In this study, recycled short carbon fibers and recycled PET were combined into a filament and used as feedstock for FFF. In order to investigate the influence of the molar mass (MM) of the rPET matrix on the mechanical performance and printability, two rPET feedstocks with a low and high MM were used to obtain CFR rPET filaments. Via extrusion, rPET filaments with a target carbon fiber content ranging from 0 to 50 wt% were processed and characterized. To verify the carbon fiber content, thermogravimetric analysis (TGA) was performed, while differential scanning calorimetry (DSC) was used to investigate the influence of the processing conditions on the degree of crystallinity of the filaments. To evaluate the effect of the carbon fibers on the shrinkage of semi-crystalline rPET, pressure-volume-temperature (pvT) measurements were carried out. Furthermore, two FFF printers which require filaments with a different diameter (i.e. 1.75 and 2.85 mm) were used to print the extruded rPET filaments. An upper limit of fiber content was determined in order to guarantee a successful printing process. And finally, the effect of the CF weight percentage on the mechanical performance was determined through tensile testing on both the filaments and printed parts.

2. Materials and Methods

2.1. Materials

The filaments produced in this study consisted of recycled materials, including mechanically recycled PET with a higher mass average MM of 21 400 g/mol (rHPET) provided by Tridea and mechanically recycled PET with a lower mass average MM of 16 800 g/mol (rLPET) from Agfa-Gevaert. Recycled unsized carbon fibers with a length of 80 to 100 μm and a diameter of 7 μm were supplied by Gen 2 Carbon, originally ELG Carbon Fibre.[42] The PET pellets were used to process filaments with a diameter of 1.75 and 2.85 mm, while the carbon fiber content varied. The rHPET pellets were used to process filaments with a target carbon fiber content ranging from 0 to 10 wt% (i.e. 10CFrHPET_{1.75} for CFR rPET filaments with 10 wt% rCFs and a diameter of 1.75 mm), while rLPET was used to obtain CFR rPET filaments with a fiber content ranging from 15 to 50 wt% (i.e. 50CFrLPET_{2.85} for CFR rPET filaments with 50 wt% rCFs and a diameter of 2.85 mm). Moreover, 1,1,1,3,3,3-hexafluoro isopropanol 99.9 % from Evochem was used for size exclusion chromatography (SEC). Furthermore, the rPET results were compared with a commercial virgin PET filament (vPET_{2.85}) by Nexeo 3D with a diameter of 2.85 mm of which the data were published in [20].

2.2. Polymer characterization

With thermogravimetric analysis (TGA), the degradation temperature and remaining carbon residue were determined using a TA Instruments Q50 operating under nitrogen atmosphere. The samples were heated from 35 to 750 $^{\circ}\text{C}$ at a heating rate of 10 $^{\circ}\text{C}/\text{min}$. The thermograms were analyzed using the TA Universal Analysis software from TA Instruments. In order to obtain modulated differential scanning calorimetry (mDSC) thermograms, a TA instrument Q2000 DSC was used, which operated under nitrogen atmosphere at a heating rate of 2 $^{\circ}\text{C}/\text{min}$, a cooling rate of 5 $^{\circ}\text{C}/\text{min}$ and modulated at ± 0.32 $^{\circ}\text{C}/\text{min}$. The analysis was performed by the TA Universal Analysis software from TA Instruments. The glass transition (T_g) and melting temperature (T_m) were determined based on the heat capacity component, i.e. the reversing heat flow of the second heating curve, while the crystallization (T_c) and cold crystallization temperature (T_{cc}) resulted from the kinetic component, i.e. the non-reversing heat flow of respectively the cooling and the second heating curve. Furthermore, the initial degree of crystallinity (X_c) was calculated via the following equation:

$$X_c (\%) = \frac{\Delta H_f - \Delta H_{cc}}{\Delta H_f^0 (1 - x)} * 100 \% \quad (1)$$

where ΔH_f is the enthalpy of fusion, ΔH_{cc} the enthalpy of cold crystallization and ΔH_f^0 the heat of fusion of 100 % crystalline PET (140 J/g), all extracted from the first heating run of respectively the reversing and non-reversing heat flow and x is the fiber mass fraction determined via TGA.[43] The mDSC measurements were performed in a temperature range between 0 $^{\circ}\text{C}$ and 300 $^{\circ}\text{C}$. Size exclusion chromatography (SEC) was performed to obtain the molar mass and the polymer dispersity. To this end, in 1.5 mL 1,1,1,3,3,3-hexafluoro isopropanol containing 0.019 % sodium trifluoroacetate, 5 mg of the PET materials was dissolved and filtered over a 0.2 μm Teflon syringe filter. For the calibration curve, poly(methyl methacrylate) standards with a molar mass ranging from 831 to 1 890 000 g/mol were used. First, a precolumn PFG combination medium with 7 μm particle size (4.6 x 30 mm) was used and thereafter two PFG combination medium microcolumns with 7 μm particle size (4.6 x 25 mm, separation range 100 – 1 000 000 g/mol) were used, in combination with a refractive index detector. The spectra were analyzed with the WinGPC UniChrom software.

2.3. Extrusion of CFR rPET filaments

To obtain CFR rPET filaments, CFR pellets were first manufactured with the twin screw Coperion compounder, which had a throughput from 2 to 10 kg/h. Before compounding, the rLPET and rHPET pellets were dried to values lower than 0.010-0.015 %. For the CFR pellets with a fiber content of 1 to 10 wt%, rHPET was compounded with the fibers which were added via a powder feeder, while for the pellets with a rCF content of 15 to 50 wt%, the rCF were mixed with rLPET before compounding and the mixture was added via the main pellet feeder. During compounding, a part of the rCF remained in the feeder, which resulted in lower actual rCF content. The compounder with 12 heating zones had a temperature profile of 230-250-265-265-270-270-280-280-285-285-285 °C, while the screws rotated at 150 rpm. A water bath was placed in between the compounder and a pelletizer which had a temperature of 30 °C. The pelletizer (Leistritz) chopped the strand at a speed of 35 m/min.

The extrusion of unreinforced and CFR rPET filaments was realized with the monofilament extrusion line (Fibre Extrusion Technology Ltd.), which has a capacity of 2.5 – 5 kg/h. The CFR rPET pellets and rHPET were dried prior to extrusion. The filament extruder had four heating zones with a temperature profile of 250-270-280-285 °C. Depending on the required filament diameter of 1.75 or 2.85 mm, the speed of the screws varied from 14 to 30 rpm respectively. Moreover, a water bath of 30 °C was placed at the end of the extruder. To obtain a consistent filament diameter and roundness, a Sikora Ecocontrol was used and depending on the obtained data, the speed and throughput was adapted to obtain the required dimensions.

2.4. Fused filament fabrication of CFR rPET

The filaments were stored in a box with controlled humidity of 20 % and a temperature of 30 °C. Herein, Prusa i3 MK3S and Ultimaker 3 were used as FFF printers, each requiring different filament diameters. The Prusa i3 MK3S requires filaments with a diameter of 1.75 mm, while the Ultimaker 3 exploits filaments with a diameter of 2.85 mm. The printing parameters are summarized in Table 1. In order to print with rPET filaments and avoid nozzle blockage, the nozzle temperature was 250 °C for the Ultimaker 3 and 260 °C for the Prusa i3 MK3S. To avoid shrinkage and warpage, a build plate temperature of 100 °C was selected for both printers, which is above the T_g . [44] The first layer of the samples was printed at half-speed (initial print speed) to ensure a good adhesion of the part to the build plate. The height of an individual deposited layer was set at 0.1 mm. The width of a deposited track was 0.35 mm. The tensile sample geometry was based on the ASTM standard D3039, while the overall length of the samples was adapted to fit the build plate. [45] Rectangular-shaped samples (165 x 25 x 2.5 mm³) with infill line pattern parallel to the load, further referred to as 0°, were printed with both FFF printers in order to examine the effect of the carbon fibers on the printing process. Furthermore, both printers had their own slicer software to convert the STL file into the corresponding G-code. Although the default settings would be identical, the G-codes would vary and therefore, the G-code was generated with the same slicer, namely the Cura 3.3.1 software.

Table 1: Summary of the printing parameters for the Prusa i3 MK3S and Ultimaker 3 printers.

Printing parameter	Prusa i3 MK3S	Ultimaker 3
Filament diameter	1.75 mm	2.85 mm
Nozzle temperature	260 °C	250 °C
Nozzle diameter	0.4 mm	0.4 mm
Build plate temperature	100 °C	100 °C
Initial print speed	20 mm/s	20 mm/s
Print speed	40 mm/s	40 mm/s
Fan cooling	100 %	100 %
Layer height	0.1 mm	0.1 mm
Track width	0.35 mm	0.35 mm
Infill line pattern	0°	0°
Infill percentage	100 %	100 %

2.5. Mechanical characterization

2.5.1. Tensile tests on filaments

The Tinius Olsen 5ST was used to perform tensile testing on the filaments. The device had a 500 N load cell and 7 filament pieces were tested within each series. The filament was placed between two clamps which exerted a pressure of 4 bar to avoid slipping. Hereafter, the crosshead had a displacement speed of 10 mm/min and proceeded until failure of the filament. The strain was calculated using the initial gage length of the filament and the crosshead displacement. The tensile modulus, ultimate tensile strength and ultimate tensile strain were calculated for each filament and significant differences ($p < 0.05$) were calculated with one-way ANOVA.

2.5.2. Tensile tests on printed parts

The measurement of the tensile properties of the printed parts was based on the ASTM standard D3039.[45] For every fixed weight percentage, at least five tensile tests were performed using an Instron 5885 machine, operated with mechanical grips and a 10 kN load cell. The printed parts were loaded at a displacement rate of 2 mm/min and until failure of the part. No end tabs were used, but thick paper was placed between the samples and the grips for protection from the grips.

A stereo digital image correlation (DIC) system (VIC-3D by Correlated Solutions with two Stingray Cameras of 5 MP and 23 mm lenses) was used to measure the full-field strain of the sample. These two cameras monitored the displacement of a black speckle pattern on a white base applied to the printed parts' surface. An image was taken every second throughout the duration of each test. The longitudinal strain of the sample was determined by a virtual extensometer. The tensile modulus was defined as the average value in the 0.1 - 0.3 % strain range. Significant differences ($p < 0.05$) were calculated with one-way ANOVA. For the calculation of the elastic properties, at least five samples were used, while for the failure properties at least three samples were used.

2.6. Pressure-volume-temperature measurements

The shrinkage during cooling was analyzed using a PVT100 (SWO Polymertechnik GmbH) according to ISO 17744.[46] Here, the samples were cooled down from 290 to 40 °C at a constant rate of 0.1 °C/s and the pressure was constant, namely 200 bar. To be able to compare with each other, the relative specific volume was plotted via normalization at 40 °C.

2.7. Scanning electron microscopy

To determine the original length of the milled carbon fibers, images were obtained by using a field emission gun scanning electron microscopy (SEM) instrument (JEOL JSM-7000F) at an acceleration voltage of 10 kV. Prior to analysis, a thin conductive gold film of approximately 20 nm was deposited on the carbon fibers by an automatic Sputter Coater K550X to avoid charging. The length of each individual carbon fiber was then determined from 10 images with ImageJ software. A total of 5113 fibers were measured.

To inspect the fracture surface, micrographs of the fractured surface after tensile testing were obtained via SEM. The images of the gold coated samples were acquired with a FEI Phenom Desktop SEM using two magnifications of 5 000 and 20 000, applying an acceleration voltage of 5 kV.

2.8. X-ray micro-computed tomography

Table 2: X-ray micro-computed tomography parameters for the extruded filaments with a target carbon fiber content of 4, 20 and 40 wt% and the CFR rPET parts printed using these filaments.

Sample	Dimensions (mm)	Image pixel size (μm)	Exposure time (ms)	Voltage (kV)	Current (μA)	Object to source distance (mm)	Number of measured fibers
4CFrHPET _{1.75}	$\varnothing = 1.75$, L = 10	0.81	1620	37	234	30.88	3425
4CFrHPET _{2.85}	$\varnothing = 2.85$, L = 10	0.88	1734	36	222	33.46	3727
20CFrLPET _{2.85}	$\varnothing = 2.85$, L = 10	0.88	1734	36	222	33.46	285
40CFrLPET _{2.85}	$\varnothing = 2.85$, L = 10	0.81	1734	36	222	30.88	569
4CFrHPET _{2.85} printed	1.3 x 3.2 x 5.0	0.88	1679	37	234	33.46	7509
20CFrLPET _{2.85} printed	1.3 x 4.4 x 4.7	0.88	1891	37	228	33.46	1936
40CFrLPET _{2.85} printed	1.2 x 4.3 x 7.8	1.28	1779	37	228	48.88	8294

To investigate fiber length and orientation distribution as well as void fraction, X-ray micro-computed tomography (μCT) scans were conducted of CFR rPET filaments and printed parts using a Bruker Skyscan 1172. Seven pristine filaments and printed parts were scanned with target fiber contents of 4 wt%, 20 wt% and 40 wt%. The scans were acquired for 180° of rotation with a rotation step of 2°. An overview of the parameters of the X-ray μCT scans is listed in Table 2. By allowing a small distance between the sample and the X-ray source, an image pixel size was reached that was small enough to detect the carbon fibers in the resin. Using the built-in reconstruction software NRecon, the reconstruction of the X-ray μCT scans was carried out. The resulting images were 4 k x 4 k pixels in size and were processed in the image processing software Avizo.

Firstly, a representative volume element (RVE) was taken inside the sample volume to crop the roughness of the outer surface. A median filter was then applied to this RVE. This filtering technique improves the results of the following processing steps such as edge detection and segmentation by removing excess noise from the images. In the next step, the fibers were selected using a greyscale threshold value that was chosen based on visual inspection. Voids were selected in the same way. Thanks to the difference in chemical contrast, the X-ray μ CT images allow to distinguish different materials based on the greyscale value of each voxel, ranging from white to black. Subsequently, a segmentation analysis was carried out, meaning that the inclusions are separated from the matrix based on the selected threshold value. The length and orientation of the inclusions were then quantified and analyzed. Inclusion length is defined as the maximum length of the Feret diameters.[47] The spatial orientation of an inclusion is calculated with the inertia moments and is described with its vector \vec{p} in a spherical coordinate system ($r = 1, \vartheta, \varphi$). Equivalently, the orientation can be described in a Cartesian coordinate system by the unit vector \vec{p} that is related to ϑ and φ :

$$\vec{p} = \begin{pmatrix} p_1 \\ p_2 \\ p_3 \end{pmatrix} = \begin{pmatrix} \sin \theta \cos \varphi \\ \sin \theta \sin \varphi \\ \cos \theta \end{pmatrix} \quad (2)$$

All inclusions that did not resemble a fiber were filtered out by using threshold values for aspect ratio, length, volume or area of the inclusion. These filters were based on expected fiber inclusions of 7 μm in average diameter, and 80 – 100 μm in average length. An overview of the amount of fibers detected and measured in each sample is given in Table 2.

The fiber length distribution (FLD) is represented with a probability density function. A description of the average fiber orientation in the samples is given by the orientation tensor, which is widely used for this purpose.[48] It is a symmetric second-order tensor and is calculated as the dyadic product of the unit vector \vec{p} . The orientation tensor A_{ij} is given in Equation (3), where n denotes the n -th fiber in the RVE. The elements of the orientation tensor represent the fiber alignment along the 1-, 2- and 3-axis. The diagonal element a_{11} for example, shows the alignment with the filament axis and the printing direction: the closer this value is to 1, the more aligned the fibers are with the printing direction.

$$A_{ij} = \begin{pmatrix} a_{11} & a_{12} & a_{13} \\ \dots & a_{22} & a_{23} \\ \dots & \dots & a_{33} \end{pmatrix} = \frac{1}{n} \sum_n (p_i p_j)_n \quad (3)$$

3. Results and discussion

3.1. Characterization of the extruded CFR rPET filaments

3.1.1. Thermal characterization and mass fraction determination

The rHPET with higher MM and rLPET pellets with lower MM were used to process filaments without carbon fibers (rHPET_{1.75} and rHPET_{2.85}) and filaments with a target carbon fiber content ranging from 1 to 10 wt% (1-10CFrHPET) and from 15 to 50 wt% (15-50CFrLPET). Two filament diameters, 1.75 and 2.85 mm, were produced. The filament diameter was measured after extrusion and ranged within 1.722 – 1.752 mm and 2.767 – 2.847 mm for the 1.75 and 2.85 mm filaments, respectively. To analyze the degradation temperature of the extruded filaments, thermogravimetric analysis (TGA) was performed on rHPET, rLPET and all extruded filaments. Table 3 provides an overview of the temperature at which the material starts disintegrating ($T_{d, \text{onset}}$). An overlay of the thermograms shows that all the rPET filaments are stable up to 350 °C and the degradation proceeds via a single step as the ester and aliphatic moieties break simultaneously (see Figure 1).[49,50] The $T_{d, \text{onset}}$ ranges

between 394 and 402 °C and it is therefore concluded that the addition of carbon fibers does not influence the degradation temperature of rPET. After decomposition, carbonized materials remain, which result from both the rPET matrix and rCF. The rCFs do not degrade before reaching 750 °C and therefore the experimental carbon fiber content can be determined by subtracting the residue of the rPET matrix from the total mass of the carbonized material. This value is then compared with the target fiber content. For a low amount of rCF (< 4 wt%), the thermograms overlap with rHPET and rHPET_{2.85} due to the low carbon fiber content. Moreover, the experimental content slightly shifted to lower values relative to the target content, which is not exceptional given the low feed rate of the powder feeder. To avoid further dosing differences during extrusion of the filaments with a target rCF content ranging from 15 to 50 wt%, the rCFs were mixed with rLPET and added via the main feeder. Blockage could not be avoided altogether, as also the hopper inlet was slightly blocked due to the large amount of fibers. Hence, also for the CFR rPET filaments with a target carbon fiber content of 40 and 50 wt%, an experimental fiber content lower than the targeted fiber contents were found for both filament diameters.

Table 3: Summary of the degradation temperature at the onset point ($T_{d, onset}$) and experimental carbon fiber content analyzed via TGA for rHPET, rLPET, the vPET filament and the extruded filaments.

Filament abbreviation	Target fiber content (wt%)	$T_{d, onset}$ (°C)	Experimental fiber content (wt%)
vPET _{2.85}	-	401	-
rHPET	-	402	-
rLPET	-	396	-
rHPET _{1.75}	0	396	-
rHPET _{2.85}	0	401	-
1CFrHPET _{1.75}	1	396	0.4
1CFrHPET _{2.85}	1	397	0.6
2CFrHPET _{1.75}	2	395	1
2CFrHPET _{2.85}	2	400	1.7
4CFrHPET _{1.75}	4	398	4.2
4CFrHPET _{2.85}	4	394	4
10CFrHPET _{1.75}	10	396	10.8
10CFrHPET _{2.85}	10	401	11.3
15CFrLPET _{1.75}	15	397	11.4
15CFrLPET _{2.85}	15	400	12.9
20CFrLPET _{1.75}	20	398	17.1
20CFrLPET _{2.85}	20	399	17.3
40CFrLPET _{1.75}	40	397	31.7
40CFrLPET _{2.85}	40	398	32.7
50CFrLPET _{1.75}	50	400	40.7
50CFrLPET _{2.85}	50	401	40.5

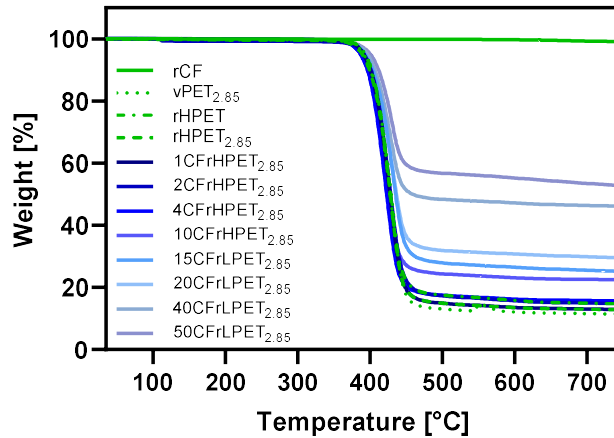


Figure 1: Schematic overview of TGA analysis performed on recycled carbon fibers (rCF), rHPET, the vPET filament and the extruded rHPET_{2.85} and CFR rPET filaments with a target carbon fiber content ranging from 1 to 50 wt% and a filament diameter of 2.85 mm.

For a complete thermal analysis, modulated differential scanning calorimetry (mDSC) of rHPET, rLPET and the extruded rPET filaments was performed to determine the glass transition (T_g), the first and second melting ($T_{m,1}$ and $T_{m,2}$) temperature, the cold crystallization (T_{cc}) and the crystallization temperature (T_c) (see Table 4). The initial degree of crystallinity (X_c) (i.e. the first heating run) is calculated through the enthalpy of fusion and cold crystallization, shown in Eq. (1).[51] It is known from literature that fillers influence the degree of crystallinity, which in turn influences the thermal properties.[34,52,53] For unreinforced rPET filaments, the crystallization temperature ranged from 201 to 203 °C. Upon addition of carbon fibers, this temperature increased to approximately 220 °C as the fillers act as nucleating agents.[34,54] Compared with the unreinforced filament rHPET_{1.75}, the degree of crystallinity of the filaments with a diameter of 1.75 mm decreased when a low amount of carbon fibers was added. The crystallinity increased towards a maximum of 14.4 % when 11.4 wt% of rCF was added. Hereafter, when the filler content increased even further, the degree of crystallinity decreased again. It can be hypothesized that a large amount of fillers could agglomerate together which hinders polymer chain mobility, lowers the nucleation effect and therefore crystallization.[34,55] Furthermore, it can be observed that the degree of crystallinity is always lower for the filaments with a diameter of 1.75 mm when compared with the filaments with a diameter of 2.85 mm. This is the result of a faster cooling after extrusion for the filaments with a smaller diameter, which results in less crystalline regions.[56] Depending on the degree of crystallinity, amorphous PET has a lower T_g of 65 °C, while for highly semi-crystalline PET, the T_g is around 92 °C.[52,57–59] Table 4 shows both the initial T_g from the first heating run ($T_{g,a}$) and the T_g of the second heating run when the thermal history is excluded ($T_{g,b}$). Here, the $T_{g,a}$ ranges from 71 to 77 °C, while $T_{g,b}$ ranges from 76 to 83 °C. Therefore, the former lower range is due to the lower X_c range (0.3 to 38.6 %) and thus the sample exhibits less crystalline regions. Here, the $T_{g,b}$ measured after removal of the thermal history is higher as more crystalline regions are formed, which is also indicated by its X_c range (from 23.3 to 48.3 %, data not shown). Nevertheless, all filaments are semi-crystalline as each shows a melting peak above 240 °C. Moreover, some filaments show two endotherms during melting, which can be attributed to two different lamella thicknesses resulting from crystallization and re-crystallization during melting.[51] As a known feature of PET, all filaments show a cold crystallization slightly above 110 °C in the first heating run, which indicates that crystals are formed just above the glass transition temperature as molecular mobility is possible.[60]

Table 4: Summary of the initial glass transition temperature ($T_{g,a}$), the glass transition temperature after removal of the thermal history ($T_{g,b}$), the (cold) crystallization temperature (T_{cc}), the melting temperatures ($T_{m,1}$ and $T_{m,2}$) and the initial degree of crystallinity (X_c) analyzed via mDSC for rHPET, rLPET, the vPET filament and the extruded filaments with a target carbon fiber content ranging from 0 to 50 wt%.

Filament	$T_{g,a}$ (°C)	$T_{g,b}$ (°C)	T_{cc} (°C)	$T_{m,1}$ (°C)	$T_{m,2}$ (°C)	T_c (°C)	X_c (%)
vPET _{2.85}	78	84	116	249	258	207	22.5
rHPET	83	83	-	241	251	201	37.6
rLPET	81	79	-	255	-	198	12.2
rHPET _{1.75}	75	81	115	243	251	201	11.8
rHPET _{2.85}	78	83	116	244	251	203	20.1
1CFrHPET _{1.75}	71	79	111	243	251	204	0.3
1CFrHPET _{2.85}	75	80	112	244	-	206	12.7
2CFrHPET _{1.75}	72	80	111	244	252	207	5.6
2CFrHPET _{2.85}	75	80	114	244	252	206	17.4
4CFrHPET _{1.75}	73	80	113	244	253	207	1.1
4CFrHPET _{2.85}	74	81	113	245	254	210	23.3
10CFrHPET _{1.75}	72	83	113	244	-	206	12.4
10CFrHPET _{2.85}	76	80	113	243	-	204	29.7
15CFrLPET _{1.75}	73	76	112	251	-	218	14.4
15CFrLPET _{2.85}	73	80	111	250	-	218	16.1
20CFrLPET _{1.75}	73	78	112	252	-	220	3.4
20CFrLPET _{2.85}	74	83	112	251	258	217	12.3
40CFrLPET _{1.75}	72	79	111	252	-	219	3.9
40CFrLPET _{2.85}	77	82	111	251	258	218	38.6
50CFrLPET _{1.75}	76	78	111	251	259	219	5.1
50CFrLPET _{2.85}	77	81	110	251	-	218	34.1

3.1.2. Size exclusion chromatography (SEC)

Mechanical recycling potentially influences the molar mass of the extruded filaments and in order to investigate how much this affects the application of low or high molar mass rPET pellets, SEC was performed on both the starting products rHPET and rLPET and the extruded filaments.[4] As shown in Table 5, the number average molar mass (M_n), the mass average molar mass (M_w) and their dispersities were determined. The data show that molar mass reduction occurs for all filaments due to thermal degradation. It is hypothesized that hydrolysis of the ester bonds due to remaining moisture was minimal as the pellets were dried at 200 °C prior to extrusion and a moisture content of 0.014 % was measured, which is below the reported 0.02 % where degradation is avoided.[61,62]

The filaments processed with rHPET showed a molar mass reduction in between 22.4 and 39.3 % as the M_w of the starting product, rHPET, was 21 400 g/mol. Furthermore, also the filaments which started from rLPET with a lower M_w of 16 800 g/mol exhibited a polymer degradation ranging from 22.6 to 33.3 %. Therefore, it can be concluded that the compounding and extrusion processes resulted in an equal polymer degradation for all filaments irrespective of the molar mass of rPET and the amount of carbon fibers added. The dispersities of all materials ranged from 1.9 to 2.4, which is a common dispersity range for PET synthesized via step-growth reaction.[63]

Table 5: Overview of the molar masses and dispersities determined by SEC for rHPET, rLPET, the vPET filament and the extruded filaments with a target carbon fiber content ranging from 0 to 50 wt%, dissolved in 1,1,1,3,3,3-hexafluoro isopropanol.

Filament	M_n (g/mol)	M_w (g/mol)	\bar{D}
vPET _{2.85}	8 500	18 000	2.1
rHPET	7 500	21 400	2.9
rLPET	7 500	16 800	2.2
rHPET _{1.75}	7 300	14 300	2.0
rHPET _{2.85}	8 500	16 600	2.0
1CFrHPET _{1.75}	6 700	15 400	2.3
1CFrHPET _{2.85}	6 000	13 000	2.2
2CFrHPET _{1.75}	8 300	15 900	1.9
2CFrHPET _{2.85}	6 400	13 800	2.1
4CFrHPET _{1.75}	7 000	15 400	2.2
4CFrHPET _{2.85}	6 100	13 100	2.1
10CFrHPET _{1.75}	6 300	14 900	2.4
10CFrHPET _{2.85}	6 600	15 700	2.4
15CFrLPET _{1.75}	5 800	12 300	2.1
15CFrLPET _{2.85}	6 300	12 600	2.0
20CFrLPET _{1.75}	6 000	12 500	2.1
20CFrLPET _{2.85}	6 600	12 800	1.9
40CFrLPET _{1.75}	5 500	12 200	2.2
40CFrLPET _{2.85}	6 900	13 000	1.9
50CFrLPET _{1.75}	5 700	11 400	2.0
50CFrLPET _{2.85}	5 100	11 200	2.2

3.1.3. Pressure-volume-temperature (pvT) measurements

The ability of carbon fibers to reduce shrinkage was investigated through pressure-volume-temperature (pvT) measurements, as it is known that semi-crystalline filaments are prone to shrinkage and warpage after printing.[35–37] When the deposited thermoplastic cools down, the free volume decreases, which is more pronounced for semi-crystalline filaments as the formed crystals are denser compared to amorphous filaments.[34]

Figure 2 shows the specific volume of rPET pellets and filaments when the temperature decreases from 290 °C to 40 °C, while the pressure was fixed. All the tested rPET pellets and filaments showed the same decreasing tendency for the specific volume, namely a linear decrease until the crystallization temperature T_c with thereafter a large decrease in volume due to the formation of dense crystals during crystallization up to its T_g . As the relative specific volume is plotted, the shrinkage of rHPET, rLPET and the extruded rPET filaments without fibers can be compared with the CFR rPET filaments. When the materials were cooled from 290 °C, a shrinkage of 17.7 % was observed for the unreinforced materials, which is the result of a decreasing polymer chain mobility (approx. 13 %) and crystallization (approx. 5 %). The fact that the shrinkage was similar was expected since the same material was used although processed differently. The similar shrinkage also showed that the rPET shrinkage is independent of the molar mass of the filament. From the moment carbon fibers were incorporated, the shrinkage reduced as those fibers fill up the free volume and prevent movement of the macromolecular rPET chains.[21,35,38,39] Indeed, 4CFrHPET_{2.85}, 15CFrLPET_{2.85} and 50CFrLPET_{2.85} showed a lower shrinkage of respectively 17.3, 16.9 and 10.3 %. Moreover, the coefficient of thermal expansion (CTE) could be calculated in the range of 50 to 70 °C (see Figure 2). The CTE of rHPET, rLPET

and rHPET_{2.85} are in agreement with literature which performed thermal expansion measurements on virgin PET.[41,64] Furthermore, it is noticed that the CTE decreased upon addition of CFs due to movement limitations. It is noticed that the shrinkage reduction is approximately equal to the concentration of the incorporated carbon fibers (i.e. shrinkage reduction of 41.8 % when 40.5 wt% carbon fibers were added). Besides a shrinkage reduction when carbon fibers were incorporated in the rPET matrix, Table 4 showed that the crystallization temperature of rPET increased, which is also noticed in . The latter will be an advantage during FFF as crystallization starts earlier upon deposition of the rPET track, which will minimize the drastic specific volume change.[38] Spörk *et al.* already reported on pvT measurements on semi-crystalline PP and amorphous ABS.[65] As the relative specific volume was plotted in that work, the rPET results could be compared, showing the same trend as for semi-crystalline PP.

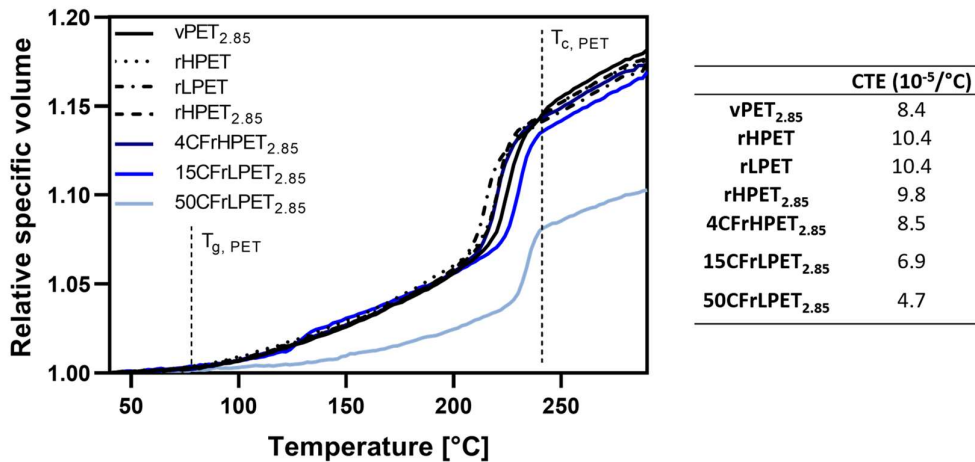


Figure 2: (Left) Schematic overview of the pvT analyses on the starting pellets rHPET, rLPET, the vPET filament and the extruded filaments with a target carbon fiber content of 0, 4, 15 and 50 wt% and a filament diameter of 2.85 mm. (Right) Overview of the coefficient of thermal expansion (CTE) calculated from pvT measurements in the region from 50 to 70 °C, which is below the T_g of PET (i.e. 80 °C).

Polymer shrinkage and warpage during cooling should be avoided in FFF as the printed part will bend and detach from the build plate.[34,66] In order to enable a sufficient adhesion to the build plate, the build plate temperature could be set slightly above the T_g, which decreases the surface tension (i.e. 100 °C for rPET as T_g ranges between 70 and 80 °C).[37,44] Besides adding fibers, shrinkage can also be reduced by blending the semi-crystalline material with another (amorphous) material or through polymer modification (i.e. incorporating side chains or influencing tacticity).[39,59–61] In the present work, it can be concluded via pvT measurements that the addition of carbon fibers to the rPET matrix resulted in a decreased shrinkage of 41.8 % when 40.5 wt% fibers were added.

3.1.4. Mechanical characterization via tensile testing

To investigate the effect of the carbon fiber content on the mechanical performance of the extruded filaments, tensile tests were carried out on the filaments. The effect of the molar mass of the polymer on the mechanical properties was checked by comparing rHPET and rLPET based filaments with similar carbon fiber weight fractions. The filaments were elongated until failure and benchmarked against rHPET_{1.75} and rHPET_{2.85}. The average tensile modulus, ultimate tensile strength and ultimate tensile strain of 7 filaments were calculated. All results are shown in Table 6. All filaments showed a sudden brittle fracture, except for the filaments with no reinforcement or lower carbon fiber target content (1 – 4 wt% and 15 wt%).

Table 6: Overview of the tensile modulus, ultimate tensile strength and strain of the vPET filament and the extruded rPET filaments with a target carbon fiber content ranging from 0 to 50 wt%.

Filament	Tensile modulus (GPa)	Ultimate tensile strength (MPa)	Ultimate tensile strain (%)
vPET _{2.85}	1.49 ± 0.12	44.91 ± 2.64	420.01 ± 45.29
rHPET _{1.75}	1.51 ± 0.18	45.49 ± 2.95	362.33 ± 15.31
rHPET _{2.85}	1.47 ± 0.08	43.31 ± 2.74	408.01 ± 60.62
1CFrHPET _{1.75}	1.86 ± 0.14	55.07 ± 2.79	149.55 ± 93.97
1CFrHPET _{2.85}	1.62 ± 0.13	40.34 ± 3.67	77.74 ± 33.11
2CFrHPET _{1.75}	2.32 ± 0.14	57.56 ± 2.65	68.60 ± 14.16
2CFrHPET _{2.85}	1.60 ± 0.19	49.50 ± 1.56	69.61 ± 40.00
4CFrHPET _{1.75}	2.59 ± 0.14	54.61 ± 5.68	6.71 ± 1.11
4CFrHPET _{2.85}	1.96 ± 0.13	52.83 ± 1.14	12.16 ± 1.74
10CFrHPET _{1.75}	4.16 ± 0.56	73.97 ± 5.26	4.09 ± 0.84
10CFrHPET _{2.85}	2.72 ± 0.54	70.57 ± 2.46	5.38 ± 1.60
15CFrLPET _{1.75}	2.44 ± 0.16	43.51 ± 6.03	4.11 ± 1.19
15CFrLPET _{2.85}	2.18 ± 0.21	47.40 ± 2.87	4.84 ± 1.12
20CFrLPET _{1.75}	3.32 ± 0.17	55.93 ± 1.45	3.35 ± 0.43
20CFrLPET _{2.85}	2.63 ± 0.16	56.06 ± 4.81	5.20 ± 2.22
40CFrLPET _{1.75}	4.86 ± 0.45	71.39 ± 2.52	2.82 ± 0.28
40CFrLPET _{2.85}	3.20 ± 0.45	64.68 ± 2.86	3.96 ± 1.03
50CFrLPET _{1.75}	6.38 ± 0.95	79.01 ± 5.29	2.39 ± 0.52
50CFrLPET _{2.85}	3.75 ± 0.40	74.13 ± 4.31	3.39 ± 0.50

The tensile modulus and strength of the filaments increase with increasing carbon fiber content, both when using rHPET and rLPET. Furthermore, as the fraction of carbon fibers increases, the ultimate strain decreases. A significant difference is observed between the 1.75 mm and 2.85 mm filaments, with the 1.75 mm filament consistently showing larger improvements in modulus, seen in Figure 3. With the addition of approximately 40 wt% fibers, the modulus is improved with 323 % for the 1.75 mm filament and only 155 % for the 2.85 mm filaments. However, the improvements in strength are similar for both fiber diameters.

The influence of the molar mass on the mechanical properties was checked for the 10CFrHPET and 15CFrLPET samples for both filament diameters. A significant drop in modulus and strength occurred when using the lower molar mass rLPET matrix instead of the rHPET matrix at an almost constant fiber weight fraction. The molar mass of the matrix dropped with 17 % between the 10CFrHPET_{1.75} and 15CFrLPET_{1.75} samples, and 20 % between the 10CFrHPET_{2.85} and 15CFrLPET_{2.85} samples (see Table 5). As the fiber weight fraction of the samples remained approximately equal, the decrease in modulus and strength is attributed to the reduction in molar mass and corresponding lower amount of chain entanglements. The drop in modulus is more severe for the 1.75 mm filament with 41 % compared to 20 % for the 2.85 mm filament. The rHPET matrix shows a superior performance compared to the rLPET matrix. This data indicates that the molar mass is important to consider when a high modulus is desired for filaments to ensure the mechanical performance of the printed part.[12]

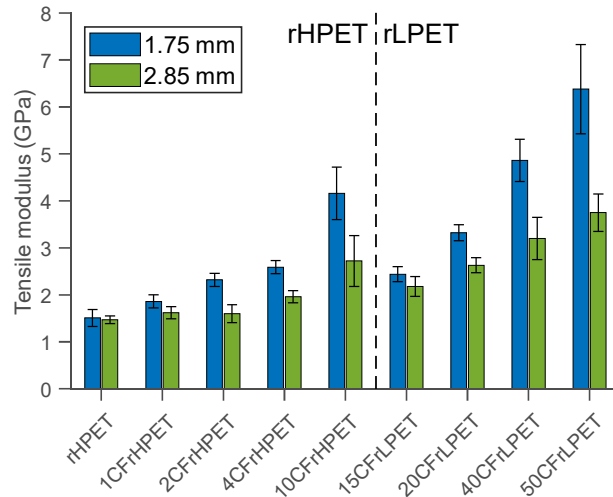


Figure 3: Overview of the tensile moduli of the extruded (CFR) rPET filaments with a diameter of 1.75 and 2.85 mm obtained via tensile testing.

3.2. Fused filament fabrication with CFR rPET filaments

3.2.1. Effect of printing process on carbon fiber length, orientation and void content

Using X-ray μ CT images, the fiber length and fiber orientation in the CFR filaments and printed parts were characterized. Figure 4 shows a rendered image of the fibers in the 4CFrHPET_{2.85} filament, produced from the X-ray μ CT scans. The X-ray μ CT images were also examined to determine the 3D void content of the printed parts, as voids can act as stress concentrators and lead to premature failure.

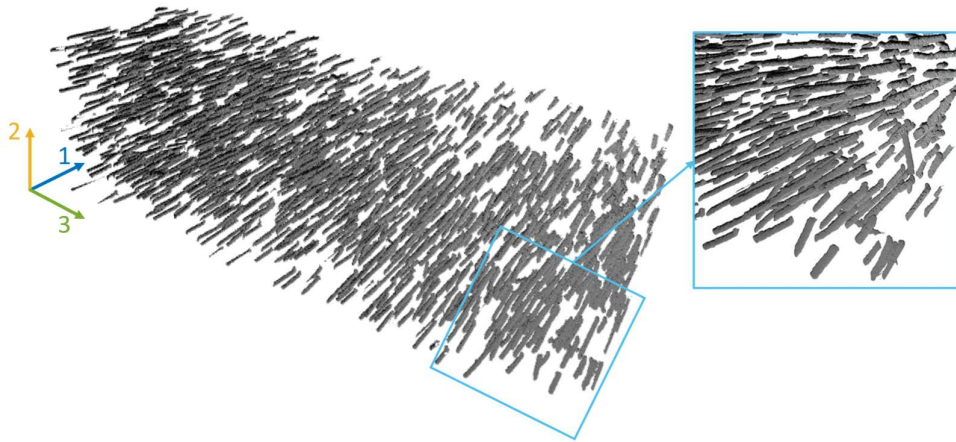


Figure 4: Rendered image obtained from X-ray μ CT scans showing the fibers inside a selected volume of a 4CFrHPET_{2.85} filament. The coordinate system (1,2,3) in which the orientation tensor is defined, is indicated.

Figure 5 shows the voids in two different cross-sections of the parts printed with the 4CFrHPET_{2.85}, 20CFrLPET_{2.85} and 40CFrLPET_{2.85} filaments. The cross-section parallel to the build plate is shown on the left and displays the voids within one layer. The cross-section perpendicular to the build plate and to the longitudinal direction of the tracks, is shown on the right and displays the voids in subsequent layers. A void fraction of 8 %, 19 %, and 14 % was found for the samples with a fiber content of 4 wt%, 17 wt% and 33 wt% respectively. The formation of these voids is driven by melt flow characteristics, like pressure and velocity gradients, but also depends on melt solidification parameters like cooling rate.[31] Voids can originate from moisture released during printing or from air entrapped during

extrusion of the filament.[17,23] The 20CFrLPET_{2.85} part contained very large voids that in some locations even cover the width of the entire track. Consequently, the sample was considered to be of poor quality. The large void fraction in the sample has also led to a reduced amount of fibers detected during processing of the X-ray μ CT images, compared to the other samples. Furthermore, the images show that the void morphology was affected by the fiber content. The sample with a target fiber weight content of 40 wt% showed a high number of much smaller voids, while the sample with a target fiber weight content of 4 wt% showed smaller voids on the track interfaces, and larger voids that appeared more scattered over the cross-section. This correlation between fiber content and void morphology has been described before in literature.[24,67] Increasing fiber content has been reported to lead to a better packing of the tracks and hence smaller voids between them. But with a rising number of fiber ends, the number of voids caused by poor interfacial bonding between fiber and matrix, increased too. Fibers can also lead to inconsistent fusion between tracks, and hence drive interfacial void formation.[23]

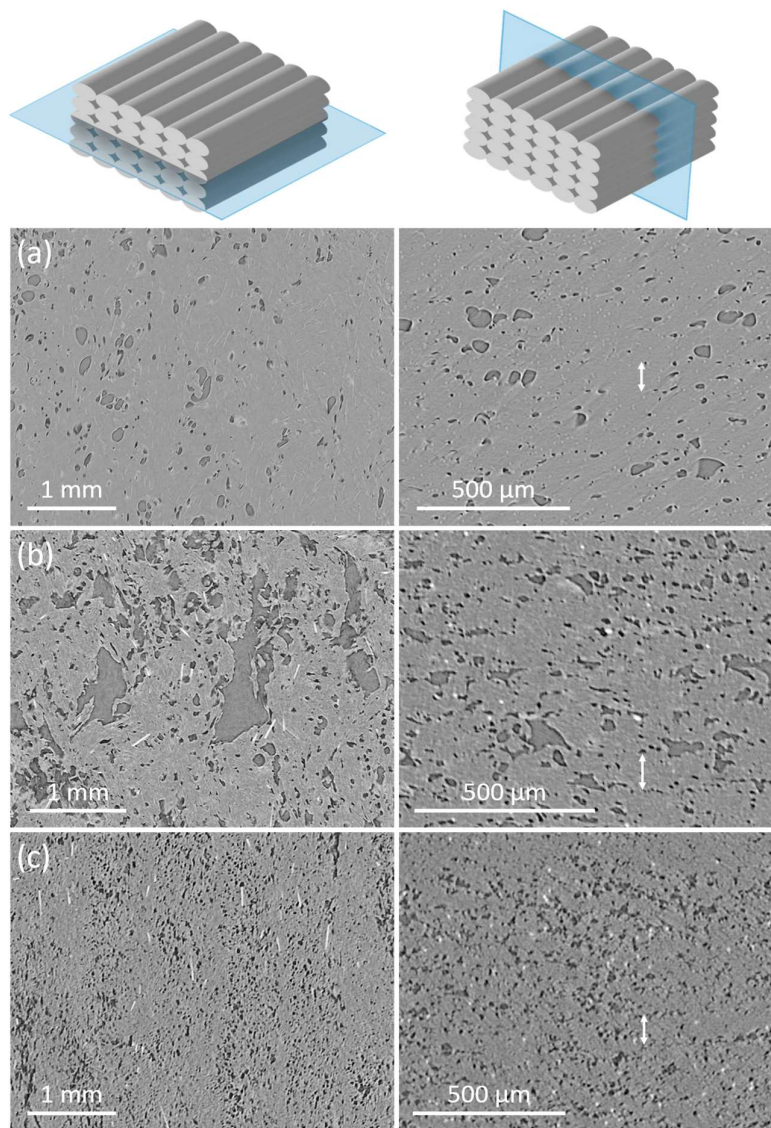


Figure 5: Void content in a CFR rPET sample printed using the (a) 4CFrHPET_{2.85}, (b) 20CFrLPET_{2.85} and (c) 40CFrLPET_{2.85} filaments, visualized through X-ray micro-computed tomography. On the left, the cross-section parallel to the build plate is shown. On the right, the cross-section perpendicular to the build plate and to the longitudinal direction of the filaments is shown. Arrows indicate the 100 μ m layer height.

As fiber length can be affected by the high shear forces involved in the manufacturing of the reinforced printed parts, the residual fiber length after extrusion and after printing was determined. The initial fiber length distribution was measured by dispersing the fibers on a tape for inspection in the SEM. The effect of extrusion and printing on the fiber length distribution, compared with the original fiber length distribution, is illustrated in Figure 6. The length distribution of the original fibers was broad, with a peak around 85 μm . After filament extrusion, the fiber length distributions reached a maximum between 73 and 87 μm for the inspected filaments. Fiber weight fraction and filament diameter did not seem to greatly affect the fiber length.

But during the printing process, the relatively long fibers (>100 μm) got substantially shortened, leading to an increased proportion of shorter fibers in the printed parts. This was likely due to the high shear forces inside the printer nozzle. Here, the fiber weight fraction did affect the measured fiber length. The parts with a fiber fraction of around 17 wt% and 33 wt%, showed substantially shorter fibers than the parts reinforced with only 4 wt% fibers. This result could be explained by the interactions of the fibers with other fibers, with the matrix, and with the walls of the narrow extruder nozzle. The number of interactions increases with fiber content, leading to more extensive fiber breakage. The decrease in fiber length with increasing fiber content has been described before in literature.[25,32,68] However, in literature it has been reported that the average length reduction in the nozzle appears limited. Yang *et al.* reports that fiber lengths are somewhat affected during printing, explained by the collisions with the nozzle wall, but no severe fiber breakage is observed.[32] Jiang and Smith have also measured only a slight reduction in weight average fiber length after deposition compared with the filament.[25]

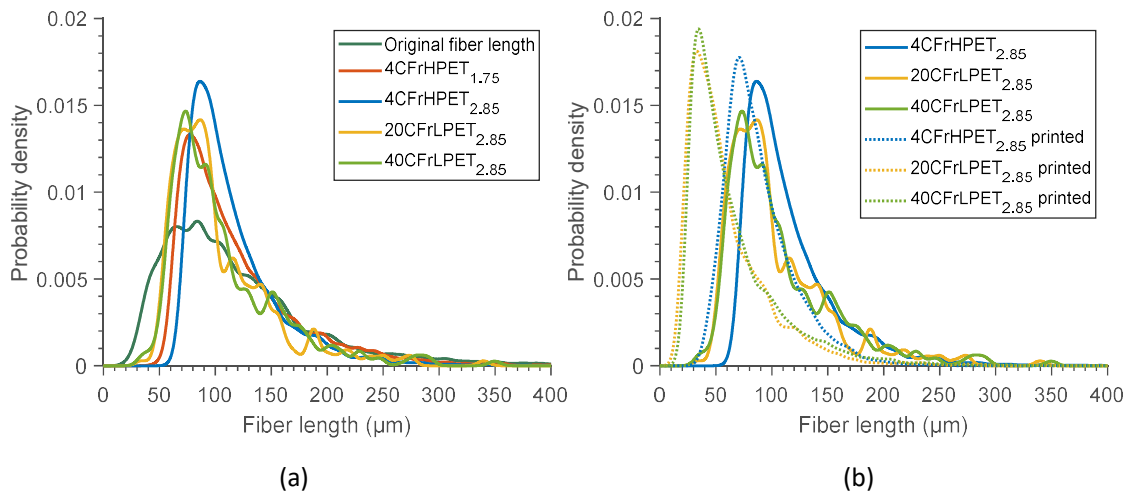


Figure 6: Fiber length probability density distributions for (a) the original fibers compared with the CFR filaments, and (b) the CFR filaments compared with the printed parts.

Table 7: Overview of the second-order orientation tensors of the CFR filaments and printed parts.

Sample	Second-order orientation tensor					
	a_{11}	a_{12}	a_{13}	a_{22}	a_{23}	a_{33}
4CFrHPET_{1.75}	0.9915	-0.0027	-0.0150	0.0031	-0.0003	0.0054
4CFrHPET_{2.85}	0.9915	-0.0030	0.0143	0.0036	-0.3298	0.0049
20CFrHPET_{2.85}	0.9880	-0.0118	0.0013	0.0049	-0.0014	0.0070
40CFrHPET_{2.85}	0.9810	-0.0074	-0.0060	0.0098	0.0005	0.0092
4CFrHPET_{2.85} printed	0.7408	0.0248	0.0160	0.2369	0.0496	0.0224
20CFrHPET_{2.85} printed	0.6322	0.2398	0.0201	0.1980	0.0042	0.1698
40CFrHPET_{2.85} printed	0.6128	0.0102	0.0041	0.3562	0.0737	0.0310

The X-ray images were also analyzed to determine the effects of printing on the fiber orientation. It is described in literature that fibers tend to be oriented along the printing direction due to the shear stress imposed on the melt during the extrusion of the feedstock filament itself, or during the extrusion of the filament in the printer nozzle.[26–29]

The average orientation of the carbon fibers in the samples was quantified by calculating the orientation tensors, given in Table 7. Figure 7 shows a representative volume of the μ CT samples with the coordinate system in which the orientation tensors are defined. The diagonal components of the tensor a_{11} , a_{22} and a_{33} denote the fiber orientations along the 1-, 2- and 3-axis respectively. In the filaments, the orientation vector along the 1-axis, which is parallel to the filament axis, was almost equal to 1, while the orientation vectors along the 2-axis and 3-axis remained small. This indicates that almost all fibers were aligned with the direction of the filament. In the printed parts at the same fiber content, the orientation vector along the 1-axis, which here was parallel to the printing direction, reaches around 0.61 – 0.74. This means that the fibers in the printed parts were still mostly oriented along the printing direction, but the extremely high alignment that was reached in the filaments was partially lost upon printing. While the a_{11} component decreased compared to the a_{11} component of the filament, the a_{22} and a_{33} components increased, indicating that the fibers tended to slightly align along the 2-axis and 3-axis. The misalignment likely occurred during deposition of the extrudate on the printing bed, as previously described by Yang et al.[32] The relative motion between the nozzle and build plate disturbs the flow field and affects the orientation of the fibers in the deposited extrudate. Furthermore, for both the filaments and the printed parts, the a_{11} component decreased with increasing fiber content. The reduction in alignment was modest for the filaments: a_{11} was 0.9915 and 0.9810 for the filaments containing 4 wt% CFs and 32.7 wt% CFs respectively. However, the reduction was more drastic for the printed parts: a_{11} was 0.7408 and 0.6128 for the printed parts containing 4 wt% CFs and 32.7 wt% CFs respectively. This data shows that a high degree of orientation of the milled fibers in rPET can be achieved through 3D printing, as previously reported for CFR ABS, PA6 and epoxy.[24,32,68]

In conclusion, the effect of increasing fiber content on the internal morphology of the CFR rPET composite was studied using X-ray μ CT imaging. The data shows that increasing fiber content changes void morphology, leading to a high number of small voids. In terms of the fibers, the data indicates the occurrence of substantial fiber breakage for higher fiber weight fractions. Finally, it was found that high fiber alignment can be achieved due to the inherent characteristics of 3D printing.

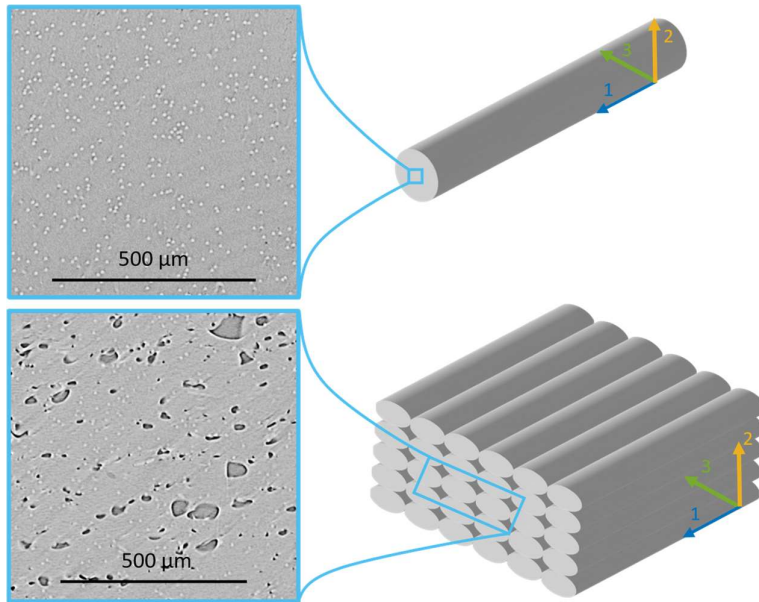


Figure 7: Illustration of a representative volume of the 4CFrHPET_{2.85} filament and printed part. A corresponding X-ray μ CT image shows the carbon fibers inside the rPET matrix for a cross-section of the filament and of the printed part.

3.2.2. Mechanical characterization of printed parts

The influence of the carbon fibers on the mechanical properties of the printed parts was investigated through tensile testing. The tensile modulus, ultimate tensile strength and ultimate tensile strain of samples printed in the loading direction with increasing fiber content are shown in Table 8. The filaments were chosen to be deposited parallel to the tensile load, in the 0° direction, as the fibers in the tracks should be aligned with the loading direction to the greatest extent possible to ensure optimal load bearing.[24] The printed reinforced parts were elongated until failure and benchmarked against rHPET_{1.75} and rHPET_{2.85}.

As was the case for the filament properties, the effect of the molar mass of the matrix on the printed part modulus was checked by comparing rHPET and rLPET based samples with similar carbon fiber weight fractions. Therefore, the performance of the 10CFrHPET and 15CFrLPET samples was examined for both filament diameters.

Table 8: Overview of the tensile modulus, ultimate tensile strength and ultimate tensile strain of the samples printed with the vPET filament and the extruded rPET filaments with a target carbon fiber content ranging from 0 to 50 wt%. Samples of which no fracture properties could be extracted ($n < 3$) are indicated with an asterisk (*).

Filament	Tensile modulus (GPa)	Ultimate tensile strength (MPa)	Ultimate tensile strain (%)
vPET _{2.85}	2.51 ± 0.16	32.6 ± 4.2	1.26 ± 0.21
rHPET _{1.75}	2.41 ± 0.04	*	*
rHPET _{2.85}	2.37 ± 0.08	*	*
1CFrHPET _{1.75}	2.70 ± 0.07	*	*
1CFrHPET _{2.85}	2.68 ± 0.24	36.9 ± 7.7	2.16 ± 0.24
2CFrHPET _{1.75}	2.81 ± 0.05	37.9 ± 2.4	1.21 ± 0.71
2CFrHPET _{2.85}	2.85 ± 0.11	29.2 ± 7.4	1.01 ± 0.31
4CFrHPET _{1.75}	3.13 ± 0.08	45.9 ± 2.0	2.53 ± 0.44
4CFrHPET _{2.85}	3.45 ± 0.15	33.9 ± 1.7	1.01 ± 0.05
10CFrHPET _{1.75}	5.41 ± 0.33	53.5 ± 1.4	2.07 ± 0.04
10CFrHPET _{2.85}	6.76 ± 0.28	64.1 ± 3.6	1.50 ± 0.24
15CFrLPET _{1.75}	4.24 ± 0.09	47.8 ± 1.9	1.76 ± 0.27
15CFrLPET _{2.85}	5.01 ± 0.35	*	*
20CFrLPET _{1.75}	5.01 ± 0.47	48.9 ± 1.0	1.65 ± 0.28
20CFrLPET _{2.85}	6.30 ± 0.63	*	*
40CFrLPET _{1.75}	7.39 ± 0.77	49.0 ± 2.2	0.80 ± 0.01
40CFrLPET _{2.85}	8.78 ± 0.21	49.5 ± 8.5	0.56 ± 0.16
50CFrLPET _{1.75}	7.66 ± 0.72	47.0 ± 0.4	0.57 ± 0.08
50CFrLPET _{2.85}	11.61 ± 0.11	58.2 ± 4.5	0.49 ± 0.07

For the samples printed with the 2.85 mm filament, an increasing tensile modulus was found upon increasing the experimental fiber content from 0.6 to 40.5 wt%. A significant improvement in tensile modulus of already 20 % was observed when only 1.7 wt% CFs were incorporated. When 40.5 wt% CFs were incorporated, an improvement of 390 % was observed.

As was the case for the filaments, a deviation from the increasing trend was observed for 15CFrLPET_{2.85}. A significant drop in modulus occurred when using the lower molar mass rLPET matrix instead of the rHPET matrix. The drop in modulus was similar for the 1.75 mm filament and 2.85 mm filament, with 22 % and 26 % respectively. This deviation is attributed to the lower molar mass of rLPET that was used for the extrusion of filaments with a fiber content of 11.4 wt% and above. It is concluded that the molar mass of the filament largely influences the mechanical properties of the printed parts. Upon incorporating more fibers in the rLPET matrix, the tensile modulus increased again to a maximum of 11.61 GPa for 50CFrLPET_{2.85}.

The failure properties of the printed parts do not show a monotonously increasing trend with increasing fiber content, as a maximum ultimate strength of 64.1 MPa was obtained for the 10CFrHPET_{2.85} samples. It is possible that the lack of an increasing trend in ultimate tensile strength could be caused by voids inside the tracks, as reported earlier for CFR ABS.[23] Adding more fibers increases the number of voids between the polymer matrix and the fibers due to the increased number of fiber ends, and also between the deposited layers as fibers can inhibit proper fusion of the deposited tracks.[23,24] Furthermore, the ultimate strain significantly decreased upon addition of

carbon fibers, even when a low amount was added. The reinforced parts failed in a brittle way, as shown in Figure 8 for 40CFrLPET_{2.85}.

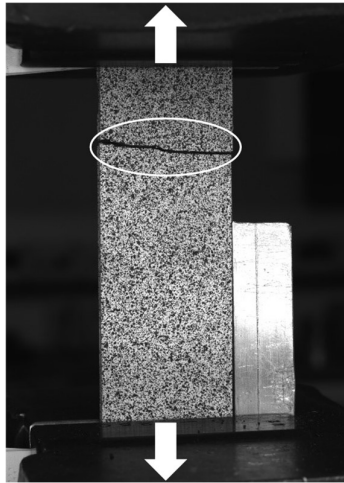


Figure 8: Brittle failure after tensile testing in a sample printed with a 40CFrLPET_{2.85} filament, indicated with a white circle. The loading direction is indicated with white arrows.

The influence of printer characteristics on the tensile modulus of printed parts was investigated by comparing the Ultimaker 3 and Prusa i3 MK3S printers, requiring the 2.85 mm and 1.75 mm filaments respectively. For the samples produced on the Prusa printer, the same increasing trend for the tensile modulus with a peak at 10 wt% was observed as for the Ultimaker samples. However, the improvement in modulus due to the addition of ± 10 wt% fibers was only 125 % for samples printed on the Prusa, which is significantly lower compared to the improvement of 185 % achieved with the Ultimaker. In literature for unreinforced rPET parts printed on different printers, a difference in modulus has been attributed to the different printer cooling control mechanisms affecting the degree of crystallinity.[20] Here, the samples printed with 10CFrHPET_{1.75} exhibited a degree of crystallinity of 8.2 %, while this was 20.6 % for the samples printed with 10CFrHPET_{2.85}. The latter showed thus more crystallites which is associated with improved modulus, also previously evidenced in literature for the semi-crystalline polymers PLA and PP.[69–71] However, for these reinforced samples, the difference in tensile modulus could also be caused by different fiber alignment or void contents in the parts. At higher fiber contents, the same trend continues. The improvement in tensile modulus for the samples with a target fiber content of 50 wt% printed on the Prusa was only 220 %, whereas an improvement of 390 % was achieved with the Ultimaker 3.

Although printing with 50CFrLPET_{1.75} and 50CFrLPET_{2.85} was successful, the print failed occasionally with both printers as the filament itself broke during printing due to its higher brittleness. For the Prusa i3 MK3S, the filament is pulled as the motor is in the extruder head, while the motor of the Ultimaker 3 is positioned behind the printing chamber so the filament is pushed into the extruder head via a tube. It can thus be deduced that filament breakage occurred independently of the motor position and diameter. When the filament was guided manually towards the motor for both printers, the filament breakage reduced drastically. Although Figure 3 in section 3.1.4. suggests that the tensile modulus could be further increased by adding more carbon fibers (> 40.7 wt%), FFF printing does not seem feasible. It can be concluded that 3D printing with rPET with a high carbon fiber content was possible, but special care is required during printing to avoid breakage of the filament. Hence, a carbon fiber content of ± 40 wt% can be considered a realistic upper limit.

The filament modulus was notably low compared to the modulus of the printed parts. This unexpected result could potentially be caused by inhomogeneities in the filament. Large voids were found in the X-ray μ CT scans of the 4CFrHPET_{1.75} and 4CFrHPET_{2.85} filaments (see Figure 9). These voids could affect the results as the measured cross-sectional area is larger than the actually loaded area, and hence the true modulus of the material is larger than the measured value.

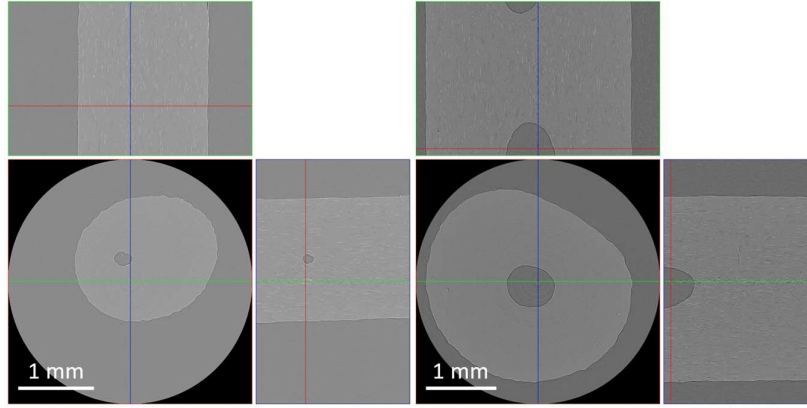


Figure 9: X-ray micro-computed tomography images of the cross-section of 4CFrHPET_{1.75} (left) and 4CFrHPET_{2.85} (right) filaments, showing large voids.

A comparison with commercial filaments is limited as important material properties such as fiber length, content and sizing are often not disclosed. Nevertheless, the mechanical performance of several commercial carbon fiber PET or PET-G composite filaments for FFF was considered for comparison with the self-extruded filament.[25,72–76] The commercial counter-parts were all based on virgin materials. In terms of stiffness, no commercial filament was found reaching the 11.61 GPa of the highly reinforced CFR rPET composite. In terms of strength, the CFR rPET composite performs equally good, or slightly less than the commercial equivalents. Future work should focus on improving the quality and strength of the CFR rPET printed part.

To conclude, improved mechanical properties were evidenced when carbon fibers were added to the rPET feedstock. Depending on the printer characteristics, an increase of 390 % for the tensile modulus was obtained when 40.5 wt% carbon fibers were incorporated into the rPET matrix. The ultimate tensile strain showed a decreasing trend when the reinforcement increased. Furthermore, a carbon content of ± 40 wt% can be considered a realistic upper limit in order to guarantee a successful printing process.

3.2.3. Fracture surface analysis

To inspect the fracture surfaces of the composite samples after tensile testing, scanning electron microscopy (SEM) images were recorded from two tensile samples printed with 10CFrHPET_{1.75} and 10CFrHPET_{2.85}.

Figure 10a and b show the fracture surface of a reinforced sample printed with 10CFrHPET_{1.75}, and 10CFrHPET_{2.85} filament respectively. Carbon fiber pull-out and the voids left by pulled-out fibers were observed in both images. As fiber pull-out rather than fiber breakage has occurred during failure in the tensile test, it appears that the interfacial bonding between the carbon fibers and the rPET matrix was not sufficient to effectively transfer the load from the matrix to the fibers. The incorporation of fibers in the polymer matrix significantly improved the mechanical performance, but to use them to their full potential, interfacial bonding should be improved or longer fibers should be used. Interfacial bonding can for example be improved through fiber surface treatment.[33] The length of the fiber is

important as optimal load transfer between matrix and fiber can only take place when a critical fiber length is exceeded.[33] The critical length of a fiber is defined as the length at which fiber failure occurs prior to the occurrence of interfacial failure, and depends on the fiber, matrix and fiber-matrix interface. This critical length can be estimated based on the Kelly model, which is a simple approximation that assumes a constant shear stress at the fiber ends.[77,78] The model exploits the interfacial shear strength between fiber and matrix (τ_i), the fiber strength (σ_{fu}), and fiber diameter (d_f) to calculate the critical fiber length (l_c), see Equation (). For CF and PET, an interfacial shear strength was found in literature.[79] Depending on the cooling rate of PET during polymer processing, an interfacial shear strength of 35 to 55 MPa was reported. The ultimate fiber strength (i.e. 4150 MPa) and fiber diameter (i.e. 7 μm) were found from the material data sheet of the manufacturer. The formula yields a critical fiber length of approximately 264 to 415 μm , much higher than the 80 - 100 μm CFs that were used.

$$l_c = \frac{\sigma_{fu}}{2\tau_i} d_f \quad (4)$$

Even though the addition of fibers improved the mechanical properties of the polymer, it can be concluded that the interfacial shear strength was either insufficient or the added fibers were too short for optimal load transfer. This finding was supported by the fiber pull-out as evidenced from SEM images, which indicated a weak interfacial adhesion, and by Kelly's formula which suggests that the fiber length exploited in this study did not exceed the critically required length for optimal load transfer.

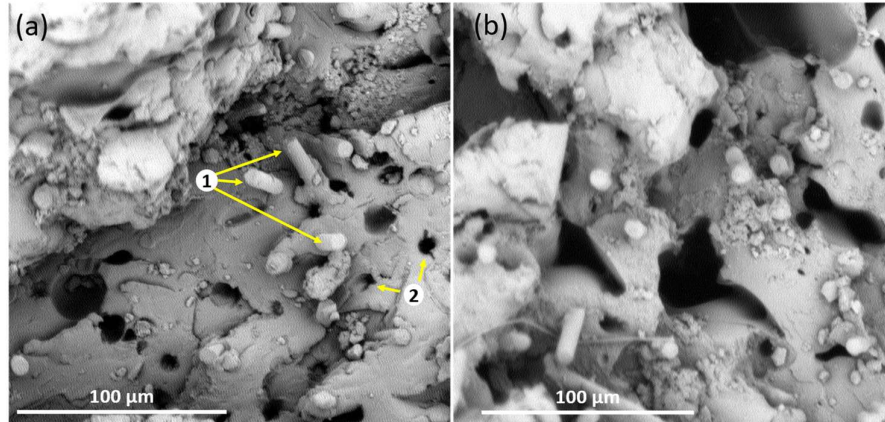


Figure 10: SEM micrographs showing the fracture surface of a (a) 10CFrHPET_{1.75} and (b) 10CFrHPET_{2.85} printed sample. Fiber pull-out (1) and the voids they left behind (2) are clearly visible, while the pulled-out fibers do not show rPET remnants, signifying poor interfacial adhesion between the fiber and matrix.

4. Conclusion

This study investigated the physico-chemical and mechanical effects on rPET filaments resulting from the incorporation of up to 40 wt% recycled carbon fibers. The results were benchmarked against an unreinforced polymer reference. Filaments of 1.75 mm and 2.85 mm in diameter were produced via melt extrusion and used as feedstock for FFF. The 1.75 mm filaments showed a lower degree of crystallinity compared to the 2.85 mm filaments, as a result of faster cooling. From SEC measurements, it could be concluded that the compounding and extrusion processes resulted in an equal polymer degradation for all filaments irrespective of the molar mass of rPET and the amount of carbon fibers

added. Via mDSC measurements, the carbon fibers were shown to act as nucleating agents, increasing the crystallization temperature with increasing fiber content. In pvT measurements, the incorporation of carbon fibers was shown to reduce rPET shrinkage up to 42 % during printing compared to unreinforced rPET. The fiber length and orientation after printing was quantified using X-ray μ CT scans. Fiber breakage after printing increased with fiber content. The extremely high fiber alignment in the filaments was only partially retained after deposition. Furthermore, the tensile properties of the filaments and the printed parts improved with increasing fiber content for both diameters. The tensile modulus improved with 390 % for the highly loaded 40.5 wt% parts. A fiber fraction of 40 wt% was found as upper limit considering blockage of fibers in compounding and processability of the filament during printing. Fiber pull-out was observed when inspecting the fracture surface via SEM images, indicating a poor interfacial adhesion between the unsized rCFs and rPET matrix. This study shows the potential of rPET to be upcycled into a filament with good processability and performance using recycled milled carbon fibers at high fiber fractions.

Acknowledgement

The authors acknowledge the support of the Agency for Innovation and Entrepreneurship Flanders via the Strategic Initiative Materials NANOFORCE research program: projects RELFICOM and PET2VALUE. The authors wish to thank Sofie Huysman for her support and advice during the extrusion of the rPET filaments performed at Centexbel.

References

1. Archana; Moses, V.; Sagar, S.; Shivraj, V.; Chetan, S. A Review on Processing of Waste PET (Polyethylene Terephthalate) Plastics. *Int. J. Polym. Sci. Eng.* **2016**, *1*, 1–13, doi:10.37628/ijpse.v1i1-2.120.
2. Scheirs, J.; Long, T.E. Modern Polyesters: Chemistry and Technology of Polyesters and Copolyesters. In *Modern Polyesters: Chemistry and Technology of Polyesters and Copolyesters*; John Wiley and Sons Ltd, 2003; pp. 1–750 ISBN 0471498564.
3. Welle, F. Twenty Years of PET Bottle to Bottle Recycling - An Overview. *Resour. Conserv. Recycl.* **2011**, *55*, 865–875.
4. Awaja, F.; Pavel, D. Recycling of PET. *Eur. Polym. J.* **2005**, *41*, 1453–1477, doi:10.1016/j.eurpolymj.2005.02.005.
5. Plastics – the Facts 2020 An Analysis of European Plastics Production, Demand and Waste Data Available online: https://plasticseurope.org/fr/wp-content/uploads/sites/2/2021/11/Plastics-the-facts-WEB-2020_versionJun21-final.pdf (accessed on 22 November 2021).
6. Paszun, D.; Spychaj, T. Chemical Recycling of Poly(Ethylene Terephthalate). **1997**.
7. Singh, A.K.; Bedi, R.; Kaith, B.S. Composite Materials Based on Recycled Polyethylene Terephthalate and Their Properties – A Comprehensive Review. *Compos. Part B Eng.* **2021**, *219*, 108928, doi:10.1016/J.COMPOSITESB.2021.108928.
8. *Recycled Polyethylene Terephthalate Market Size, Share & Trends Analysis Report By Product (Clear, Colored), By End Use (Fiber, Food & Beverage Containers & Bottles), By Region, And Segment Forecasts, 2021 - 2028*; 2021;
9. Gardan, J. Additive Manufacturing Technologies: State of the Art and Trends. *Int. J. Prod. Res.* **2016**, *54*, 3118–3132, doi:10.1080/00207543.2015.1115909.
10. Huang, Y.; Leu, M.C.; Mazumder, J.; Donmez, A. Additive Manufacturing: Current State, Future Potential, Gaps and Needs, and Recommendations. *J. Manuf. Sci. Eng. Trans. ASME* **2015**, *137*, 1–11, doi:10.1115/1.4028725.
11. Brenken, B.; Barocio, E.; Favaloro, A.; Kunc, V.; Pipes, R.B. Fused Filament Fabrication of Fiber-Reinforced Polymers: A Review. *Addit. Manuf.* **2018**, *21*, 1–16, doi:10.1016/j.addma.2018.01.002.
12. Blok, L.G.; Longana, M.L.; Yu, H.; Woods, B.K.S. An Investigation into 3D Printing of Fibre Reinforced Thermoplastic Composites. *Addit. Manuf.* **2018**, *22*, 176–186, doi:10.1016/j.addma.2018.04.039.
13. Gao, X.; Yu, N.; Li, J. Influence of Printing Parameters and Filament Quality on Structure and Properties of Polymer Composite Components Used in the Fields of Automotive. In *Structure and Properties of Additive Manufactured Polymer Components*; Elsevier, 2020; pp. 303–330.
14. Klippstein, H.; Diaz De Cerio Sanchez, A.; Hassanin, H.; Zweiri, Y.; Seneviratne, L. Fused Deposition Modeling for Unmanned Aerial Vehicles (UAVs): A Review. *Adv. Eng. Mater.* **2018**, *20*, 1700552, doi:10.1002/adem.201700552.
15. Sathies, T.; Senthil, P.; Anoop, M.S. A Review on Advancements in Applications of Fused Deposition Modelling Process. *Rapid Prototyp. J.* **2020**, *26*, 669–687.
16. Chohan, J.S.; Singh, R. Enhancing Dimensional Accuracy of FDM Based Biomedical Implant Replicas by Statistically Controlled Vapor Smoothing Process. *Prog. Addit. Manuf.* **2016**, *1*, 105–113, doi:10.1007/s40964-016-0009-4.
17. Zander, N.E.; Gillan, M.; Lambeth, R.H. Recycled Polyethylene Terephthalate as a New FFF Feedstock Material. *Addit. Manuf.* **2018**, *21*, 174–182, doi:10.1016/j.addma.2018.03.007.
18. Yang, C.; Tian, X.; Li, D.; Cao, Y.; Zhao, F.; Shi, C. Influence of Thermal Processing Conditions in 3D Printing on the Crystallinity and Mechanical Properties of PEEK Material. *J. Mater. Process. Technol.* **2017**, *248*, 1–7, doi:10.1016/j.jmatprotec.2017.04.027.

19. Baldenegro-Perez, L.A.; Navarro-Rodriguez, D.; Medellin-Rodriguez, F.J.; Hsiao, B.; Avila-Orta, C.A.; Sics, I. Molecular Weight and Crystallization Temperature Effects on Poly(Ethylene Terephthalate) (PET) Homopolymers, an Isothermal Crystallization Analysis. *Polym.* **2014**, *Vol. 6*, Pages 583–600 **2014**, *6*, 583–600, doi:10.3390/POLYM6020583.
20. Van de Voorde, B.; Katalagarianakis, A.; Huysman, S.; Toncheva, A.; Raquez, J.-M.; Duretek, I.; Holzer, C.; Cardon, L.; Bernaerts, K. V.; Van Hemelrijck, D.; et al. Effect of Extrusion and Fused Filament Fabrication Processing Parameters of Recycled Poly(Ethylene Terephthalate) on the Crystallinity and Mechanical Properties. *Addit. Manuf.* **2022**, *50*, 102518, doi:10.1016/J.ADDMA.2021.102518.
21. Love, L.J.; Kunc, V.; Rios, O.; Duty, C.E.; Elliott, A.M.; Post, B.K.; Smith, R.J.; Blue, C.A. The Importance of Carbon Fiber to Polymer Additive Manufacturing. **2014**, doi:10.1557/jmr.2014.212.
22. van de Werken, N.; Tekinalp, H.; Khanbolouki, P.; Ozcan, S.; Williams, A.; Tehrani, M. Additively Manufactured Carbon Fiber-Reinforced Composites: State of the Art and Perspective. *Addit. Manuf.* **2019**, *301*, 100962, doi:10.1016/j.addma.2019.100962.
23. Ning, F.; Cong, W.; Qiu, J.; Wei, J.; Wang, S. Additive Manufacturing of Carbon Fiber Reinforced Thermoplastic Composites Using Fused Deposition Modeling. *Compos. Part B Eng.* **2015**, *80*, 369–378, doi:10.1016/J.COMPOSITESB.2015.06.013.
24. Tekinalp, H.L.; Kunc, V.; Velez-Garcia, G.M.; Duty, C.E.; Love, L.J.; Naskar, A.K.; Blue, C.A.; Ozcan, S. Highly Oriented Carbon Fiber-Polymer Composites via Additive Manufacturing. *Compos. Sci. Technol.* **2014**, *105*, 144–150, doi:10.1016/j.compscitech.2014.10.009.
25. Jiang, D.; Smith, D.E. Anisotropic Mechanical Properties of Oriented Carbon Fiber Filled Polymer Composites Produced with Fused Filament Fabrication. *Addit. Manuf.* **2017**, *18*, 84–94, doi:10.1016/j.addma.2017.08.006.
26. Heller, B.P.; Smith, D.E.; Jack, D.A. Effects of Extrudate Swell and Nozzle Geometry on Fiber Orientation in Fused Filament Fabrication Nozzle Flow. *Addit. Manuf.* **2016**, *12*, 252–264, doi:10.1016/J.ADDMA.2016.06.005.
27. Ferreira, R.T.L.; Amatte, I.C.; Dutra, T.A.; Bürger, D. Experimental Characterization and Micrography of 3D Printed PLA and PLA Reinforced with Short Carbon Fibers. *Compos. Part B Eng.* **2017**, *124*, 88–100, doi:10.1016/J.COMPOSITESB.2017.05.013.
28. Compton, B.G.; Lewis, J.A. 3D-Printing of Lightweight Cellular Composites. *Adv. Mater.* **2014**, *26*, 5930–5935, doi:10.1002/adma.201401804.
29. Liao, G.; Li, Z.; Cheng, Y.; Xu, D.; Zhu, D.; Jiang, S.; Guo, J.; Chen, X.; Xu, G.; Zhu, Y. Properties of Oriented Carbon Fiber/Polyamide 12 Composite Parts Fabricated by Fused Deposition Modeling. *Mater. Des.* **2018**, *139*, 283–292, doi:10.1016/j.matdes.2017.11.027.
30. Zhong, W.; Li, F.; Zhang, Z.; Song, L.; Li, Z. Short Fiber Reinforced Composites for Fused Deposition Modeling. *Mater. Sci. Eng. A* **2001**, *301*, 125–130, doi:10.1016/S0921-5093(00)01810-4.
31. Papon, E.A.; Haque, A. Tensile Properties, Void Contents, Dispersion and Fracture Behaviour of 3D Printed Carbon Nanofiber Reinforced Composites. *J. Reinf. Plast. Compos.* **2018**, *37*, 381–395, doi:10.1177/0731684417750477.
32. Yang, D.; Zhang, H.; Wu, J.; McCarthy, E.D. Fibre Flow and Void Formation in 3D Printing of Short-Fibre Reinforced Thermoplastic Composites: An Experimental Benchmark Exercise. *Addit. Manuf.* **2021**, *37*, 101686, doi:10.1016/J.ADDMA.2020.101686.
33. Blok, L.; Longana, M.; Woods, B. Fabrication and Characterisation of Aligned Discontinuous Carbon Fibre Reinforced Thermoplastics as Feedstock Material for Fused Filament Fabrication. *Materials (Basel)*. **2020**, *13*, 4671, doi:10.3390/ma13204671.
34. Vaes, D.; Van Puyvelde, P. Semi-Crystalline Feedstock for Filament-Based 3D Printing of Polymers_preproof. *Prog. Polym. Sci.* **2021**, 101411, doi:10.1016/j.progpolymsci.2021.101411.

35. Spoerk, M.; Sapkota, J.; Weingrill, G.; Fischinger, T.; Arbeiter, F.; Holzer, C. Shrinkage and Warpage Optimization of Expanded-Perlite-Filled Polypropylene Composites in Extrusion-Based Additive Manufacturing. *Macromol. Mater. Eng.* **2017**, *302*, 1700143, doi:10.1002/mame.201700143.
36. Chatham, C.A.; Zawaski, C.E.; Bobbitt, D.C.; Moore, R.B.; Long, T.E.; Williams, C.B. Semi-Crystalline Polymer Blends for Material Extrusion Additive Manufacturing Printability: A Case Study with Poly(Ethylene Terephthalate) and Polypropylene. *Macromol. Mater. Eng.* **2019**, *304*, 1800764, doi:10.1002/mame.201800764.
37. Kuo, C.C.; Wu, Y.R.; Li, M.H.; Wu, H.W. Minimizing Warpage of ABS Prototypes Built with Low-Cost Fused Deposition Modeling Machine Using Developed Closed-Chamber and Optimal Process Parameters. *Int. J. Adv. Manuf. Technol.* **2019**, *101*, 593–602, doi:10.1007/s00170-018-2969-7.
38. Fischer, J.M. *Handbook of Molded Part Shrinkage and Warpage*; 2003; Vol. 6; ISBN 1-884207-72-3.
39. Kim, M.W.; Lee, S.H.; Youn, J.R. Effects of Filler Size and Content on Shrinkage and Gloss of Injection Molded PBT/PET/Talc Composites. *Polym. Compos.* **2010**, 1020–1027, doi:10.1002/pc.
40. Ferrari, F.; Corcione, C.E.; Montagna, F.; Maffezzoli, A. 3D Printing of Polymer Waste for Improving People's Awareness about Marine Litter. *Polymers (Basel)*. **2020**, *12*, 1–14, doi:10.3390/POLYM12081738.
41. Exconde, M.K.J.E.; Co, J.A.A.; Manapat, J.Z.; Magdaluyo, E.R. Materials Selection of 3D Printing Filament and Utilization of Recycled Polyethylene Terephthalate (PET) in a Redesigned Breadboard. In Proceedings of the Procedia CIRP; Elsevier B.V., January 1 2019; Vol. 84, pp. 28–32.
42. ELG Carbon Fibre Ltd. *Carbiso™ MF Milled Fibre*;
43. Blaine, R.L. *Polymer Heats of Fusion, Therm. Appl. Note*; TA Instruments, 109 Lukens Drive, New Castle DE 19720, USA, 2002;
44. Spoerk, M.; Gonzalez-Gutierrez, J.; Sapkota, J.; Schuschnigg, S.; Holzer, C. Effect of the Printing Bed Temperature on the Adhesion of Parts Produced by Fused Filament Fabrication. *Plast. Rubber Compos.* **2018**, *47*, 17–24, doi:10.1080/14658011.2017.1399531.
45. ASTM D3039 / D3039M-17, Standard Test Method for Tensile Properties of Polymer Matrix Composite Materials,.
46. ISO 17744:2004, Plastics — Determination of Specific Volume as a Function of Temperature and Pressure (PvT Diagram) — Piston Apparatus Method.
47. Merkus, H.G. *Particle Size Measurements*; Particle Technology Series; Springer Netherlands: Dordrecht, 2009; ISBN 978-1-4020-9015-8.
48. Advani, S.G.; Tucker, C.L. The Use of Tensors to Describe and Predict Fiber Orientation in Short Fiber Composites. *J. Rheol. (N. Y. N. Y.)*. **1987**, *31*, 751–784, doi:https://doi.org/10.1122/1.549945.
49. Venkatachalam, S.; Shilpa, G.N.; Jayprakash, V.L.; Prashant, R.G.; Krishna, R.; Anil, K.K. Degradation and Recyclability of Poly (Ethylene Terephthalate). In *Polyester*; 2012; pp. 75–98.
50. McNeill, I.C.; Bounekhel, M. Thermal Degradation Studies of Terephthalate Polyesters: 1. Poly(Alkylene Terephthalates). *Polym. Degrad. Stab.* **1991**, *34*, 187–204, doi:10.1016/0141-3910(91)90119-C.
51. Kong, Y.; Hay, J.N. Multiple Melting Behaviour of Poly(Ethylene Terephthalate). *Polymer (Guildf)*. **2002**, *44*, 623–633, doi:10.1016/S0032-3861(02)00814-5.
52. Alves, N.M.; Mano, J.F.; Balaguer, E.; Duen, J.M.M.; Gomez Ribelles, J.L. Glass Transition and Structural Relaxation in Semi-Crystalline Poly (Ethylene Terephthalate): A DSC Study. *Polymer (Guildf)*. **2002**, *43*, 4111–4122, doi:10.1016/S0032-3861(02)00236-7.
53. Wu, C.S.; Liao, H.T. Interface Design of Environmentally Friendly Carbon Nanotube-Filled Polyester Composites: Fabrication, Characterisation, Functionality and Application. *Express Polym. Lett.* **2017**, *11*, 187–198, doi:10.3144/expresspolymlett.2017.20.

54. Pires, L.S.O.; Fernandes, M.H.F.V.; de Oliveira, J.M.M. Crystallization Kinetics of PCL and PCL–Glass Composites for Additive Manufacturing. *J. Therm. Anal. Calorim.* **2018**, *134*, 2115–2125, doi:10.1007/s10973-018-7307-7.
55. Gnanasekaran, K.; Heijmans, T.; van Bennekom, S.; Woldhuis, H.; Wijnia, S.; de With, G.; Friedrich, H. 3D Printing of CNT- and Graphene-Based Conductive Polymer Nanocomposites by Fused Deposition Modeling. *Appl. Mater. Today* **2017**, *9*, 21–28, doi:10.1016/j.apmt.2017.04.003.
56. Um, H.J.; Hwang, Y.T.; Choi, K.H.; Kim, H.S. Effect of Crystallinity on the Mechanical Behavior of Carbon Fiber Reinforced Polyethylene-Terephthalate (CF/PET) Composites Considering Temperature Conditions. *Compos. Sci. Technol.* **2021**, *207*, 108745, doi:10.1016/J.COMPOSITECH.2021.108745.
57. Illers, K.H. Geordnete Strukturen in „Amorphem“ Polyäthylenterephthalat. *Kolloid-Zeitschrift und Zeitschrift für Polym.* **1971**, *245*, 393–398, doi:10.1007/BF01501003.
58. Demirel, B.; Yaraş, A.; Elçiçek, H. Crystallization Behavior of PET Materials. *BAÜ Fen Bil. Enst. Derg. Cilt* **2011**, *13*, 26–35.
59. Olabisi, O.; Adewale, K. *Handbook of Thermoplastics*; second.; CRC Press, 2016; ISBN 9781466577237.
60. Wellen, R.M.R.; Rabello, M.S. The Kinetics of Isothermal Cold Crystallization and Tensile Properties of Poly (Ethylene Terephthalate). *J. Mater. Sci.* **2005**, *40*, 6099–6104, doi:10.1007/s10853-005-3173-3.
61. Malik, N.; Kumar, P.; Shrivastava, S.; Ghosh, S.B. An Overview on PET Waste Recycling for Application in Packaging. *Int. J. Plast. Technol.* **2017**, *21*, 1–24, doi:10.1007/s12588-016-9164-1.
62. Scheirs, J. *Polymer Recycling: Science, Technology and Applications*; John Wiley and Sons Ltd, 1998;
63. Weisskopf, K. Characterization of Polyethylene Terephthalate by Gel Permeation Chromatography (GPC). *J. Polym. Sci. Part A Polym. Chem.* **1988**, *26*, 1919–1935, doi:10.1002/pola.1988.080260718.
64. Pereira, J.R.C.; Porter, R.S. Extrusion Drawn Amorphous and Semi- Crystalline Poly (Ethylene Terephthalate): 3 . Linear Thermal Expansion Analysis. *Polymer (Guildf)*. **1984**, *25*, 869–876, doi:10.1016/0032-3861(84)90020-X.
65. Spoerk, M. Optimisation of the Mechanical Properties and Processing of Polypropylene and Poly(Lactic Acid) Parts Produced by Extrusion-Based Additive Manufacturing, 2018.
66. Fitzharris, E.R.; Watanabe, N.; Rosen, D.W.; Shofner, M.L. Effects of Material Properties on Warpage in Fused Deposition Modeling Parts. *Int. J. Adv. Manuf. Technol.* **2018**, *95*, 2059–2070, doi:10.1007/s00170-017-1340-8.
67. Yu, S.; Hwang, Y.H.; Hwang, J.Y.; Hong, S.H. Analytical Study on the 3D-Printed Structure and Mechanical Properties of Basalt Fiber-Reinforced PLA Composites Using X-Ray Microscopy. *Compos. Sci. Technol.* **2019**, *175*, 18–27, doi:10.1016/J.COMPOSITECH.2019.03.005.
68. Hmeidat, N.S.; Elkins, D.S.; Peter, H.R.; Kumar, V.; Compton, B.G. Processing and Mechanical Characterization of Short Carbon Fiber-Reinforced Epoxy Composites for Material Extrusion Additive Manufacturing. *Compos. Part B Eng.* **2021**, *223*, 109122, doi:10.1016/J.COMPOSITESB.2021.109122.
69. Das, A.; Marnot, A.E.C.; Fallon, J.J.; Martin, S.M.; Joseph, E.G.; Bortner, M.J. Material Extrusion-Based Additive Manufacturing with Blends of Polypropylene and Hydrocarbon Resins. *ACS Appl. Polym. Mater.* **2019**, *2*, 911–921, doi:10.1021/ACSAPM.9B01127.
70. Benwood, C.; Anstey, A.; Andrzejewski, J.; Misra, M.; Mohanty, A.K. Improving the Impact Strength and Heat Resistance of 3D Printed Models: Structure, Property, and Processing Correlations during Fused Deposition Modeling (FDM) of Poly(Lactic Acid). *ACS Omega* **2018**, *3*, 4400–4411, doi:10.1021/ACSOMEGA.8B00129.
71. Wach, R.A.; Wolszczak, P.; Adamus-Wlodarczyk, A. Enhancement of Mechanical Properties of FDM-PLA Parts via Thermal Annealing. *Macromol. Mater. Eng.* **2018**, *303*, 1800169, doi:10.1002/MAME.201800169.

72. BASF Technical Data Sheet Ultrafuse PET CF15. **2019**.
73. LUVOCOM 3F PET CF 9780 BK.
74. RECREUS PET-G CF.
75. Essentium PET-CF. **2020**.
76. Bigrep PET-CF Available online: <https://bigrep.com/filaments/pet-cf/> (accessed on 4 August 2022).
77. Lacroix, T.; Tiimans, B.; Keunings, R.; Desaeger, M.; Verpoest, I. Modelling of Critical Fibre Length and Interfacial Debonding in the Fragmentation Testing of Polymer Composites. *Compos. Sci. Technol.* **1992**, *43*, 379–387.
78. Folkes, M.J.; Wong, W.K. Determination of Interfacial Shear Strength in Fibre-Reinforced Thermoplastic Composites. *Polymer (Guildf)*. **1987**, *28*, 1309–1314, doi:10.1016/0032-3861(87)90443-5.
79. Ye, L.; Scheuring, T.; Friedrich, K. Matrix Morphology and Fibre Pull-out Strength of T700/PPS and T700/PET Thermoplastic Composites. *J. Mater. Sci.* **1995**, *30*, 4761–4769, doi:10.1007/BF01154482.